BeadNet: a network for automated spherical marker detection in radiographs for geometry calibration

V. Nguyen[1], J. De Beenhouwer[1], S. Bazrafkan[1], A-T. Hoang[2], S. Van Wassenbergh[3], J. Sijbers[1]
[1] imec - Vision Lab, Department of Physics, University of Antwerp, Belgium
[2] DiSTA, University of Insubria, Italy
[3] Functional Morphology Lab, University of Antwerp, Belgium

***Abstract*—Spherical markers are commonly used by phantom-based calibration methods for X-ray CT systems. Defining the position of the marker centers is therefore crucial to estimate the geometry parameters accurately. Although marker bearing structures are often built from materials of low X-ray attenuation, they still overlap with the marker in projection images. This complicates accurate determination of the marker centers.**
In this work, we explore the technique of Deep Learning to extract the marker center coordinates from the calibration projections. By training a Deep Learning network for each marker center coordinate, 2D positions of the marker are derived. With simulated as well as real experiments, it is shown that the trained Deep Learning networks can be used to accurately estimate the marker positions, and hence also the geometry of the X-ray CT system.

***Index Terms*—Deep Learning, calibration, cone-beam CT.**

I. Introduction

X-ray CT geometry calibration using phantoms often relies on spherical markers to calibrate the geometry parameters. In general, calibration procedures align the analytically calculated markers' orbits with the centers extracted from the calibration phantom radiographs, it is therefore important to define the centers of the markers on the calibration projection as accurately as possible. Several effects caused by the cone-beam X-ray geometry that hinder the extraction of the marker center positions were addressed in the work of Desbat et al. [1] including magnification, stretch, and asymmetrical factors. Desbat et al. [1] addressed three possible factors that generate asymmetrical marker projections in the X-ray radiographs. In that study, the calibration radiographs were first segmented to obtain the binary images containing the marker regions only. Marker centroids were calculated as center-of-masses of the marker regions. Sawyer et al. [2] located the marker centers by fitting a Gaussian and a projection of a sphere for corresponding marker projections. In both works, X-ray attenuation of the marker bearing structure on the projection data, was not taken into account. It was also difficult to accurately segment or to fit a fitting function for asymmetrical marker regions.
In the work presented by Liu et al. [3], the marker centers were extracted by firstly applying a grey-value threshold to remove non-marker structure as much as possible. Afterwards, several iterations of erosion followed by dilation filters were applied to remove narrow stripes of the supporting material. Finally, a circular Hough transform was used to locate the center of each marker on the X-ray radiograph. The procedure requires the diameters of the markers to be known.
In our previous work [4], we presented a technique based on the normalized cross correlation (NCC) between the markers and a template to define region-of-interests (ROIs) around the markers on the calibration data. This was followed by a subsample matching process to locate the center of the markers more precisely. The extracted center positions were then used to calibrate a real X-ray CT system [5].
In this paper, we propose Deep Learning to extract the calibration marker centers for which two neural networks are trained separately for each of 2D center coordinates on the projection. We validate our method on simulated and experimental calibration use cases and compare to the conventional NCC approach. The paper is structured as follows. Section II presents our methodology to generate the training dataset along with the process to extract the bead centers accurately using BeadNet. Section III discusses the simulation experiments that were performed to validate our proposed procedure as well as the experiments and results using real LEGO phantom datasets. Finally, further discussion and conclusions are presented in section IV.

II. Methodology

A. Geometry estimation

Fig. 1 shows the stereoscopic X-ray system used in this study: The 3-Dimensional DYnamic MOrphology using X-rays (3D^{2}YMOX) system that is designed for morphological and biomechanical research on animals [5]. Fig. 2 demonstrates the LEGO phantom (Fig. 2a) and its X-ray radiograph acquired with the 3D^{2}YMOX system (Fig. 2b). The geometry of this modular system can be described by six parameters to parameterize detector translations $\left\{\Delta x^d, \Delta y^d, \Delta z^d\right\}$ and detector orientations $\left\{\theta^d, \phi^d, \eta^d\right\}$ in 3D space.
In addition, six more parameters were needed to define the object's orientations $\{\theta^o, \phi^o, \eta^o\}$ and translations $\{\Delta x^o, \Delta y^o, \Delta z^o\}$ with respect to the rotation axis coordinate system. As has been discussed in [4], the geometry calibration procedure involved iteratively minimizing the total Euclidean norm between the reference and measured coordinates across all projections and marker centers. Knowledge of the position of the marker centers is key for accurate estimation of the X-ray system's geometry.

Fig. 1. The 3D^{2}YMOX system.

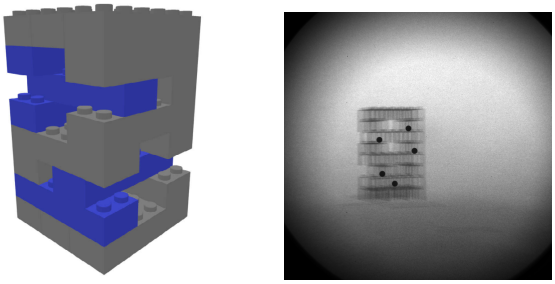

(a) (b)

Fig. 2. A real LEGO calibration phantom (a) and its X-ray projection from the 3D^{2}YMOX system (b).

B. BeadNet

In the conventional method [4], the center of each bead is estimated from the center-of-mass (COM) of its corresponding region of interest (ROI), which is extracted from the calibration projections. However, cone-beam effects and the overlapping projection of the holding structure on the ROIs complicate the COM calculation. It calls for a robust method that can handle different cone-beam geometry effects as well as asymmetric ROIs and derive center locations more accurately.

The center estimation procedure can be described as finding a mapping model F that takes the marker ROIs $\boldsymbol{x}$ as inputs with parameters $\boldsymbol{W}$ and returns the corresponding center coordinates. $\boldsymbol{W}$ is obtained through an optimization process that minimizes the difference between $F(\boldsymbol{x}, \{\boldsymbol{W}\})$ and ground-truth center coordinates (u^{gt}, v^{gt}).

$$\hat{\boldsymbol{W}} = \arg\min_{\boldsymbol{W}} \left\{ \left[F(\boldsymbol{x}, \{\boldsymbol{W}\}) - (u', v') \right]^2 \right\} \qquad (1)$$

In Eq. (1), F represents any Deep Learning model that learns abstract features from the input ROIs and maps them to the center coordinates of the bead in the ROI considering t being the hyperbolic tangent function and $t(u^{gt}) = u'$, $t(v^{gt}) = v'$. Two Deep Learning models (BeadNet) were trained separately for each center coordinate regression. The goal of BeadNet is to find a suitable abstract feature to map a marker ROI to its corresponding center coordinates. Choosing a feature learning model is important to have accurate center inference. Resnet-50 [6] emerges as a Deep Learning model that is trained on more than million images for object classifications. Resnet-50 is 50 layers deep and is divided into five convolution layers. We exploited the robustness of the pre-trained Resnet-50 model in learning object abstract features to continue training for our marker center extraction. To this end, two BeadNets were trained at a learning rate of 0.01 using an adaptive learning rate optimizer with a batch size of 40 ROIs.

Strategy to generate training dataset

The generation of training data is one of the key steps for applications of Deep Learning. The X-ray energy spectrum can be different for each acquisition. Hence, the training dataset included projections of the calibration phantom simulated with different X-ray source spectra. Moreover, as the cone-beam X-ray CT system was parameterized using 12 degrees-of-freedom, the training dataset needs to mimic a variety of possible geometry configurations, which are common settings of the 3D^{2}YMOX system. A set of 400 projections were simulated for each of 120 angles covering 360° rotation. For each set, the object and detector orientations and translations were modified by a random value generated from a uniform distribution in the intervals of $[-10, 10]^\circ$ and $[-30, 30]$ mm, respectively. The object yaw ϕ^o was generated randomly up to 200° simulating varied orientations of the calibration phantom. A 1100 mm source-detector distance (SDD) along with varied source-object distances (SODs) were simulated for typical positions of the sources, the object, and the detectors of the 3D^{2}YMOX system.

Reference marker center orbits that correspond to the simulated geometries were calculated analytically with which 25 ROIs were extracted around each marker from every simulated radiograph using reference marker positions. The training dataset contains the marker ROIs and their corresponding ground-truth center coordinates. In this work, the ROIs were at a size of 39×39 pixels that mainly cover center patches of the marker projections.

III. Experiments and Results

A. Generation of experimental datasets

The training and simulated datasets were generated using the LEGO phantom STL models and the ASTRA CAD projector toolbox [7]. The system vector geometry was calculated with respect to the geometry misalignment parameters for every projection angle using the ASTRA Toolbox [8], [9]. Then, the ASTRA CAD projector simulated X-ray radiographs of the phantom with a 150 keV polychromatic spectrum, the predefined vector geometries, and a detector pixel size of 142 μm, which corresponds to the pixel size of the 3D^{2}YMOX system.

The validation dataset containing 44 simulated sets were generated mimicking different X-ray cone-beam geometries. Corresponding marker ROIs along with the initial marker center coordinates were extracted to feed the trained BeadNets so as to estimate the center coordinates more accurately. Two more simulated datasets were generated for 3D CT reconstruction evaluations including a set of the calibration phantom and a set of a test phantom projections. These two

datasets were simulated with the same detector translation and orientation parameters but different randomly generated object positions and orientations.

Validation of BeadNet using simulated datasets

The bead centers were extracted from the validation

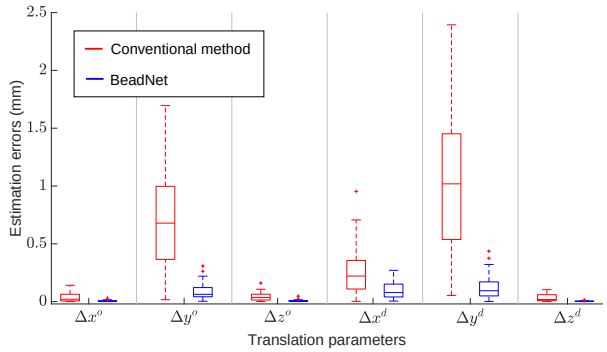

(a)

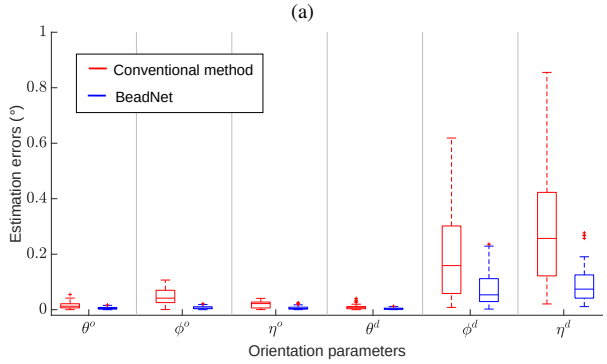

(b)

Fig. 3. Estimation errors of the translation (a) and the orientation (b) parameters using the conventional method (red) and BeadNet (blue) to extract the marker centers.

dataset with conventional NCC method and BeadNet. From the extracted bead trajectories, the X-ray system's geometry was then estimated. Fig. 3 shows the geometry estimation errors from the NCC and BeadNet method. As shown in this figure, the geometry parameters are more accurately estimated when relying on the BeadNet marker center estimates compared to NCC based estimation. The translation parameters are calibrated with average errors of 130 μm from BeadNet method, while conventional method yields mean error of up to 1000 μm. The orientation parameters are also estimated close to the GTs by BeadNet inferred marker centers with mean error of less than 0.1° while mean error from conventional method is of 0.25°. These estimates show that BeadNet yields accurate marker positions for geometry calibration.

Reconstruction from simulated phantom projections

In practice, multiple objects are usually scanned in a same geometry setting. That is, the sources and detectors are placed in a fixed position in terms of the detector

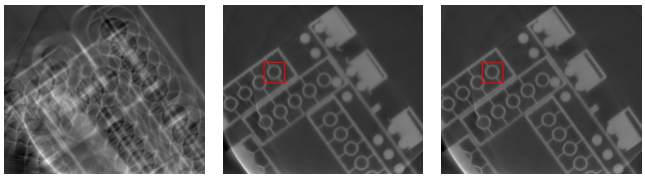

(a) (b) (c)

Fig. 4. Cross-sections of the reconstructed volume using simulated phantom dataset before (a) and after geometry calibration with the conventional technique (b) and BeadNet (c). Zoomed versions from the red squares are shown in Fig. 5.

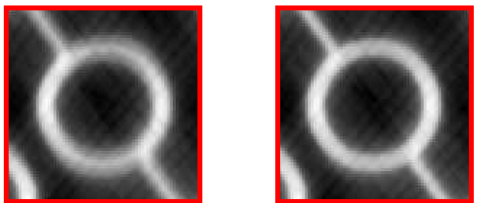

(a) (b)

Fig. 5. With the conventional method, misalignment artifacts still appear at the edges of the bricks in the reconstruction (a), while the artifacts are substantially reduced in the CT slice using BeadNet (b).

translations $\{\Delta x^d, \Delta y^d, \Delta z^d\}$ and orientations $\{\theta^d, \phi^d, \eta^d\}$ in the acquisition while the target objects are altered to acquire different datasets. The geometry was calibrated with the calibration phantom dataset for the reconstruction a test phantom, which was also built from LEGO bricks, to assess 3D CT quality and to anticipate the artifacts caused by the remaining geometry misalignments.

Fig. 4 shows the cross-sections of a real phantom reconstruction before (Fig. 4a) and after (Fig. 4b, Fig. 4c) geometry alignment. The vertical translation of the detector Δy^d was estimated more accurately using the marker orbits obtained with BeadNet. This is why the two axial slices shown in Fig. 4b and in 4c do not coincide but are shifted vertically in the 3D CT volumes. Apparent artifacts can be observed in the reconstructed slices before correcting the geometry (Fig. 4a), while the brick structure is clearly revealed in Fig. 4b and 4c. These images demonstrate that the misaligned geometry was substantially compensated in the reconstruction.

Reconstruction from real test phantom projections

The geometry of the 3D^{2}YMOX system was calibrated with a real LEGO phantom. The calibration data were firstly flatfield and log corrected before they were undistorted to remove the pincushion distortion due to the intensifier curvature [10], and the sigmoidal distortion caused by the magnetic field generated during the stage rotation [11]. The bead center trajectories were extracted by the conventional method and BeadNet, and used to estimate the geometry parameters.

In this validation, the geometry was corrected for the misalignments before reconstructing a real test dataset obtained in the same geometric configuration with that the calibration projections were acquired. Fig. 6 shows the

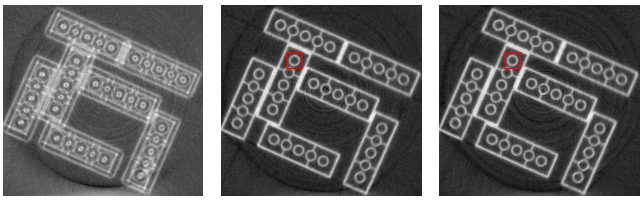

(a) (b) (c)

Fig. 6. Cross-sections extracted from the reconstructions of a LEGO test phantom before (a) and after geometry calibration using conventional method (b) and BeadNet (c) to extract the marker centers. Without compensating the geometry misalignment, the internal brick structures are distorted (a). In (b, c), the artifacts are considerably reduced revealing sharp edges and apparent shapes of the LEGO bricks. Moreover, the artifacts are better suppressed in (c) than in (b) as highlighted in red and shown in Fig. 7b and Fig. 7a, respectively.

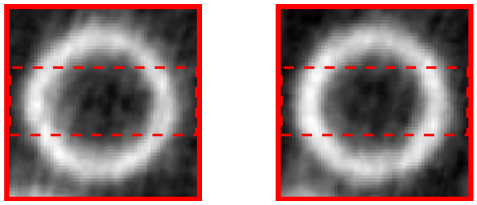

(a) (b)

Fig. 7. Misalignment artifacts still appear at the edges of the LEGO bricks and distort the shapes in the conventional method (a), while the edges are better recovered and sharper in the CT slice using BeadNet (b).

reconstructed slices of the test phantom before (Fig. 6a) and after (Fig. 6b, Fig. 6c) calibration. The reconstructed volume before compensating the geometry misalignment suffered from severe artifacts in the form of blurred edges of the LEGO bricks. In Fig. 6b and Fig. 6c, however, the shapes and edges of the bricks are well recovered in the reconstruction. This demonstrates that our estimation algorithm is capable of calibrating a real X-ray CT system. Moreover, the artifacts are better suppressed in Fig. 6c than in Fig. 6b as highlighted in red and displayed in Fig. 7a and Fig. 7b, respectively. Additionally, Fig. 8 shows the accumulated intensity profiles that were plotted through the center rows (dashed red) in the ROIs Fig. 7a and Fig. 7b from the conventional NCC method (orange) and BeadNet (blue). The line plots indicate that the contrast was slightly improved in the reconstruction from BeadNet method.

IV. Discussion & conclusion

In this paper, we presented a robust method to extract the centers of the spherical calibration markers on the X-ray radiographs using Deep Learning. Simulation experiments demonstrated that BeadNet can deliver better estimation of the marker centers and consequently the geometry parameters were estimated more accurately. After geometry misalignment correction, the misalignment artifacts were significantly suppressed from the 3D CT volume. From the marker center orbits extracted by BeadNet the geometry parameters are calibrated, and hence we obtain better quality of the CT reconstructions compared to the results with conventional NCC method. The reconstruction from the real datasets acquired from the

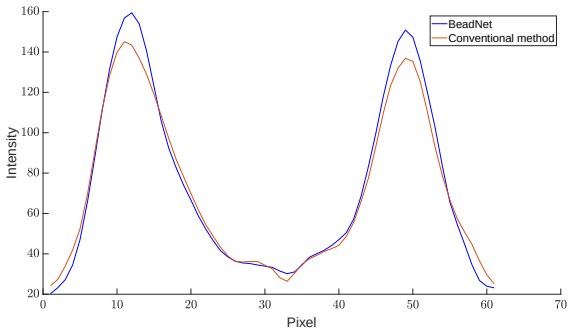

Fig. 8. Intensity profiles plotted through the rows (dashed boxes) in Fig. 7a and Fig. 7b.

3D^{2}YMOX system demonstrated that BeadNet can accurately extract the center of the markers on the real X-ray projections.

Acknowledgements

This work has been supported by the University Research Fund, UAntwerp BOF-GOA 2016 33927, the Research Foundation - Flanders (FWO) SBO project MetroFlex (S004217N), and the Flemish Government (AI Vlaanderen programme).

References

[1] L. Desbat, R. Clackdoyle, L. Grezes-Besset, C. Mennessier, and I. Bricault, “Cone-beam imaging of delta functions,” in *IEEE Nuclear Science Symposium Conference Record*, vol. 5. IEEE, 2006, pp. 2859–2863.

[2] S. A. Sawyer and E. C. Frey, “Practical improvement of geometric parameter estimation for cone beam microCT imaging,” in *IEEE Nuclear Science Symposium Conference Record*, vol. 4. IEEE, 2005, pp. 2315–2319.

[3] Y. Liu, “Improve industrial cone-beam computed tomography by integrating prior information,” Ph.D. dissertation, ETH Zurich, 2001.

[4] V. Nguyen, J. De Beenhouwer, J. Sanctorum, S. Van Wassenbergh, P. Aerts, J. J. J. Dirckx, and J. Sijbers, “A low-cost and easy-to-use phantom for cone-beam geometry calibration of a tomographic X-ray system,” *9th Conference on Industrial Computed Tomography, (iCT 2019)*, pp. 1–8, 2019.

[5] 3D2YMOX, 2018-06-19, 3-Dimensional DYnamic MOrphology using X-rays. [Online]. Available: https://www.uantwerpen.be/en/research-groups/3d2ymox/

[6] K. He, X. Zhang, S. Ren, and J. Sun, “Deep residual learning for image recognition,” in *Proceedings of the IEEE Computer Society Conference on Computer Vision and Pattern Recognition*, vol. 2016-December, 2016, pp. 770–778.

[7] A. Marinovszki, J. De Beenhouwer, and J. Sijbers, “An efficient CAD projector for X-ray projection based 3D inspection with the ASTRA Toolbox,” in *8th Conference on Industrial Computed Tomography*, 2018.

[8] W. Van Aarle, W. J. Palenstijn, J. Cant, E. Janssens, F. Bleichrodt, A. Dabravolski, J. De Beenhouwer, K. J. Batenburg, and J. Sijbers, “Fast and flexible X-ray tomography using the ASTRA toolbox,” *Optics Express*, vol. 24, no. 22, pp. 25 129–25 147, 2016.

[9] W. Van Aarle, W. J. Palenstijn, J. De Beenhouwer, T. Altantzis, S. Bals, K. J. Batenburg, and J. Sijbers, “The ASTRA Toolbox: A platform for advanced algorithm development in electron tomography,” *Ultramicroscopy*, vol. 157, no. 2015, pp. 35–47, 2015.

[10] J. G. Sanctorum, D. Adriaens, J. J. J. Dirckx, J. Sijbers, C. Van Ginneken, P. Aerts, and S. Van Wassenbergh, “Methods for characterization and optimisation of measuring performance of stereoscopic x-ray systems with image intensifiers,” *Measurement Science and Technology*, vol. 30, no. 10, p. 105701, 2019.

[11] J. G. Sanctorum, V. Nguyen, J. Sijbers, S. Van Wassenbergh, and J. J. J. Dirckx, “Projection angle adapted distortion correction in high-speed image-intensifier based tomography,” in *6th International Conference on Image Formation in X-Ray Computed Tomography*, 2020.